Modeling the inherent optical properties of the ocean based on the detailed composition of the planktonic community

Dariusz Stramski, Annick Bricaud, and André Morel

We describe an approach to modeling the ocean's inherent optical properties (IOPs) that permits extensive analyses of IOPs as the detailed composition of suspended particulate matter is varied in a controlled manner. Example simulations of the IOP model, which includes 18 planktonic components covering a size range from submicrometer viruses and heterotrophic bacteria to microplanktonic species of 30-μm cell diameter, are discussed. Input data to the model include the spectral optical cross sections on a per particle basis and the particle-number concentration for each individual component. This approach represents a significant departure from traditional IOP and bio-optical models in which the composition of seawater is described in terms of a few components only or chlorophyll concentration alone. The simulations illustrate how the separation and understanding of the effects of various types of particle present within a water body can be achieved. In an example simulation representing an oligotrophic water body with a chlorophyll a concentration of 0.18 mg m^{-3}, the planktonic microorganisms altogether are the dominant particulate component in the process of light absorption, but their relative contribution to light scattering is smaller than that of nonliving particles. A series of simulations of water bodies with the same chlorophyll a concentration but dominated by different phytoplankton species shows that composition of the planktonic community is an important source of optical variability in the ocean.

OCIS codes: 010.0010, 010.4450.

1. Introduction

Current models describing the relationships between the optical properties of the upper ocean and seawater components are often based on a parameterization of seawater composition in terms of the concentration of chlorophyll a, which is a principal pigment in phytoplankton. This approach evolved from numerous observations that showed that changes in the concentration of chlorophyll a (Chl) are accompanied by more or less systematic variations in the inherent optical properties (IOPs) and apparent optical properties (AOPs) of the upper ocean, especially if a sufficiently wide range of Chl values in so-called case 1 waters is considered.[1–4] The empirical correlation between Chl and optical properties has formed the basis of bio-optical models that can be used to predict IOPs and AOPs given Chl, or vice versa, including the retrieval of Chl from remote-sensing reflectance $R_{rs}(\lambda)$ (λ is the light wavelength). Recent studies in bio-optical oceanography and ocean color remote sensing have often been focused on such correlation models.[5–7]

In reality, however, the overly simplified parameterization of seawater composition in terms of Chl alone does not account for much of the optical variability observed in natural waters. Because there is a wide variety of optically significant organic and inorganic materials whose concentrations within natural water bodies are highly variable, any particular measured IOP or AOP can frequently differ by tens or even hundreds of percent from the value predicted by a chlorophyll-based model, and similar errors can occur when Chl is being predicted from an IOP or AOP. The errors can be exceptionally large in waters in which optical properties depend considerably on suspended and dissolved materials that do not covary with phytoplankton pigment concentration. The

D. Stramski (stramski@mpl.ucsd.edu) is with the Marine Physical Laboratory, Scripps Institution of Oceanography, University of California at San Diego, La Jolla, California 92093-0238. A. Bricaud and A. Morel are with the Laboratoire de Physique et Chimie Marines, Centre National de la Recherche Scientifique, Université Pierre et Marie Curie, B.P. 8, 06238 Villefranche-sur-Mer, France.
Received 29 June 2000; revised manuscript received 31 January 2001.
0003-6935/01/182929-17$15.00/0

waters with a significant degree of noncovariation between Chl and other water constituents are typically (albeit not only) encountered in coastal areas and are referred to as case 2 waters.[3]

The bulk inherent optical properties of a water body result from additive contributions associated with all individual water components that absorb and scatter light. The additive property of IOP's has long been utilized to represent the mix of suspended and dissolved materials in optical modeling, but these descriptions have been typically limited to only two or three components in addition to pure water itself.[8–11] Dissolved organic matter, which includes a complex group of compounds varying in molecular size and chemical composition, is one of the components that affect light absorption.[12,13] Suspended matter, which is extremely diverse in origin, composition, and optical properties, has been usually described in terms of two components or a single component representing the cumulative optical effect of all suspended particles. The two particulate components that have been most commonly used in the additive IOP equations are the chlorophyll-bearing phytoplankton and detritus.[14–16] Suspended minerals were identified as a separate particulate component in some optical models of inland waters.[17–19]

In the common approach based on the restricted number of components, a water body is considered with no regard as to the species composition of the planktonic community, types of mineral particle, and nonliving organic matter. This limitation can be important to optical modeling and understanding of the optical variability observed in natural waters. For example, it has been shown that two water bodies with an identical chlorophyll concentration and an identical particle composition with the sole exception of the difference in the relative proportions of the concentration of small (~1-μm) and larger (~8-μm) phytoplankton cells exhibit significantly different optical properties.[20] Although a complete optical model incorporating each and every individual component of seawater is clearly unattainable, this example illustrates the need to accommodate more components that would provide a more realistic (but still approximate) model. One important challenge is to advance our understanding of how variations in the detailed composition of planktonic community affect the ocean's optical properties.

Here we describe an approach to modeling the bulk inherent optical properties of a water body that permits extensive analyses of IOPs as the detailed composition of the planktonic community is varied in a controlled manner. We discuss example simulations of the IOP model, which includes 18 planktonic components covering a size range from submicrometer viruses and heterotrophic bacteria to microplanktonic species 30 μm in cell diameter. Organic detritus, mineral particles, and air bubbles are also considered in the simulations with the purpose of providing approximate background values of the IOPs associated with these components. Input data to the model include the spectral optical cross sections on a per particle basis and a particle-number concentration for each individual component. This input is distinctive because the individual components in the existing IOP models have been typically described by using the mass-specific optical coefficients and the concentration of the components expressed in terms of mass per unit volume of water.[11]

2. Formulation of the Inherent Optical Property Model

The total inherent optical properties of a water body, the absorption coefficient $a(\lambda)$, the scattering coefficient $b(\lambda)$, the backscattering coefficient $b_b(\lambda)$, the beam attenuation coefficient $c(\lambda)$, and the volume-scattering function $\beta(\Psi, \lambda)$ are all the sums of the relevant bulk IOP's associated with each of the various components of a water body.[8–11] Thus the sum of the absorption coefficients of the water itself, of each planktonic component, and of any other absorbing component present in the water, such as detritus, mineral particles, and colored dissolved organic matter, yields the total absorption coefficient $a(\lambda)$ of a water body. Similarly, corresponding sums of all contributions attributable to components that are significant in terms of light scattering give the total $\beta(\Psi, \lambda)$, $b(\lambda)$, and $b_b(\lambda)$. The total beam attenuation $c(\lambda)$ is the sum of $a(\lambda)$ and $b(\lambda)$.

The additive equation for the absorption coefficient in our model is written as

$$\begin{aligned} a(\lambda) &= a_w(\lambda) + \sum_{i=1}^{18} a_{\mathrm{pla},i}(\lambda + a_{\mathrm{det}}(\lambda) + a_{\mathrm{min}}(\lambda) + a_{\mathrm{CDOM}}(\lambda) \\ &= a_w(\lambda) + \sum_{i=1}^{18} N_{\mathrm{pla},i}\sigma_{a,\mathrm{pla},i}(\lambda) + N_{\mathrm{det}}\sigma_{a,\mathrm{det}}(\lambda) \\ &\quad + N_{\mathrm{min}}\sigma_{a,\mathrm{min}}(\lambda) + a_{\mathrm{CDOM}}(\lambda), \end{aligned} \tag{1}$$

where $a_w(\lambda)$ is the absorption coefficient of pure water,[21] $a_{\mathrm{pla},i}(\lambda)$ is the absorption coefficient of the ith planktonic component, $a_{\mathrm{det}}(\lambda)$ is the absorption coefficient of the detrital particles, $a_{\mathrm{min}}(\lambda)$ is the absorption coefficient of mineral particles, and $a_{\mathrm{CDOM}}(\lambda)$ is the absorption coefficient of colored dissolved organic matter. All these coefficients have units of inverse meters. The contributions of particulate components in Eq. (1) are expressed in terms of the product of the number concentration of particles N (units, m^{-3}) and the absorption cross section on a per particle basis $\sigma_a(\lambda)$ (units, m^2).

Equation (1) includes 18 planktonic components, which are described in detail below. The absorption contribution for each planktonic component $a_{\mathrm{pla},i}(\lambda)$ is written as a product of the number of planktonic cells per unit volume of water $N_{\mathrm{pla},i}$ and the single-particle absorption cross section of the average cell $\sigma_{a,\mathrm{pla},i}(\lambda)$. Similarly, the detrital and mineral absorption coefficients, $a_{\mathrm{det}}(\lambda)$ and $a_{\mathrm{min}}(\lambda)$, are determined as a product of the total concentration, N_{det} or N_{min}, and the average absorption cross sections, $\sigma_{a,\mathrm{det}}(\lambda)$ or $\sigma_{a,\mathrm{min}}(\lambda)$, of the respective components. Finally, Eq. (1) includes $a_{\mathrm{CDOM}}(\lambda)$, which can be modeled in terms of the exponential function of λ.[12] However, because the focus of this study is on par-

ticulate components, we omit $a_{\mathrm{CDOM}}(\lambda)$ from further consideration.

Equations analogous to Eq. (1) can be written for $b(\lambda)$, $c(\lambda)$, and $b_b(\lambda)$. For example, the total scattering coefficient is

$$\begin{aligned} b(\lambda) &= b_w(\lambda) + \sum_{i=1}^{18} b_{\mathrm{pla},i}(\lambda) + b_{\mathrm{det}}(\lambda) + b_{\mathrm{min}}(\lambda) + b_{\mathrm{bub}}(\lambda) \\ &= b_w(\lambda) + \sum_{i=1}^{18} N_{\mathrm{pla},i}\sigma_{b,\mathrm{pla},i}(\lambda) + N_{\mathrm{det}}\sigma_{b,\mathrm{det}}(\lambda) \\ &\quad + N_{\mathrm{min}}\sigma_{b,\mathrm{min}}(\lambda) + N_{\mathrm{bub}}\sigma_{b,\mathrm{bub}}(\lambda), \end{aligned} \tag{2}$$

where $b_w(\lambda)$, $b_{\mathrm{pla},i}(\lambda)$, $b_{\mathrm{det}}(\lambda)$, $b_{\mathrm{min}}(\lambda)$, and $b_{\mathrm{bub}}(\lambda)$ are the scattering coefficients of pure seawater,[22] the ith planktonic component, detrital particles, mineral particles, and air bubbles, respectively. We calculated these component scattering coefficients by using the scattering cross sections of the various components, $\sigma_{b,\mathrm{pla},i}(\lambda)$, $\sigma_{b,\mathrm{det}}(\lambda)$, $\sigma_{b,\mathrm{min}}(\lambda)$, and $\sigma_{b,\mathrm{bub}}(\lambda)$, and the component concentrations in the water. Note that bubbles are assumed to be nonabsorbing and are not included in Eq. (1). The dissolved organic matter is assumed to make a negligible contribution to scattering and is therefore omitted from Eq. (2). Analogous to Eq. (2), the total backscattering coefficient $b_b(\lambda)$, which represents the integrated scattering effect at scattering angles Ψ from 90° to 180°, is formulated with the use of backscattering cross sections, $\sigma_{bb,\mathrm{pla},i}(\lambda)$, $\sigma_{bb,\mathrm{det}}(\lambda)$, $\sigma_{bb,\mathrm{min}}(\lambda)$, and $\sigma_{bb,\mathrm{bub}}(\lambda)$, and component concentrations in water.

The total volume-scattering function $\beta(\Psi, \lambda)$, in units of $\mathrm{m}^{-1}\ \mathrm{sr}^{-1}$, is likewise a sum of contributions associated with various components:

$$\begin{aligned} \beta(\psi, \lambda) &= \beta_w(\psi, \lambda) + \sum_{i=1}^{18} \beta_{\mathrm{pla},i}(\psi, \lambda) + \beta_{\mathrm{det}}(\psi, \lambda) \\ &\quad + \beta_{\mathrm{min}}(\psi, \lambda) + \beta_{\mathrm{bub}}(\psi, \lambda) \\ &= b(\lambda)\tilde{\beta}(\psi, \lambda) \\ &= b_w(\lambda)\tilde{\beta}_w(\psi, \lambda) + \sum_{i=1}^{18} b_{\mathrm{pla},i}(\lambda)\tilde{\beta}_{\mathrm{pla},i}(\psi, \lambda) \\ &\quad + b_{\mathrm{det}}(\lambda)\tilde{\beta}_{\mathrm{det}}(\psi, \lambda) + b_{\mathrm{min}}(\lambda)\tilde{\beta}_{\mathrm{min}}(\psi, \lambda) \\ &\quad + b_{\mathrm{bub}}(\lambda)\tilde{\beta}_{\mathrm{bub}}(\psi, \lambda). \end{aligned} \tag{3}$$

where Ψ is the scattering angle ranging from 0° to 180° and $\beta_w(\Psi, \lambda)$, $\beta_{\mathrm{pla},i}(\Psi, \lambda)$, $\beta_{\mathrm{det}}(\Psi, \lambda)$, $\beta_{\mathrm{min}}(\Psi, \lambda)$, and $\beta_{\mathrm{bub}}(\Psi, \lambda)$ are the volume-scattering functions of pure seawater, the ith planktonic component, detritus, mineral particles, and air bubbles, respectively. As shown in Eq. (3) these component scattering functions are determined as the product of the component scattering coefficients and the component scattering phase functions. For example, for the ith planktonic component, we have

$$\beta_{\mathrm{pla},i}(\psi, \lambda) = b_{\mathrm{pla},i}(\lambda)\tilde{\beta}_{\mathrm{pla},i}(\psi, \lambda), \tag{4}$$

where $\tilde{\beta}_{\mathrm{pla},i}(\Psi, \lambda)$, in units of sr^{-1}, is the scattering phase function of the ith planktonic component.

Next we describe the optical properties of various particulate components that are used as input to example simulations of this model.

3. Optical Properties of Planktonic Organisms

In Table 1 we provide 18 planktonic components, each representing a particular group or species of microorganism considered in this study. Values for the average cell size, real and imaginary indices of refraction, and chlorophyll a content of each component are also given in Table 1. Data that characterize the optical properties of these planktonic components were derived from eight studies that involved laboratory measurements of bacterial and phytoplankton cultures and modeling of particle optics.[23–30] Viruses are the only component for which data are based on modeling alone, that is, Mie-scattering calculations for realistic approximations to the size distribution and refractive index of viral particles.[25] Heterotrophic bacteria represent a multispecies assemblage of these microbes, and three other components, PROC, SYNE, and SYMA, result from averaging different strains or species as indicated in Table 1. The remaining nanophytoplankton and microphytoplankton components are represented by a single species ranging in particle size from ~4 to 30 μm.

The design of the experiments, the conditions in which the cultures were grown, and the sampling strategy differed among the eight selected studies, which is described in detail in the original references.[23–30] The selection of these studies for this research was based on the following criterion: The suite of measurements performed on planktonic cultures must have included, as a minimum requirement, the spectral beam attenuation coefficient $c(\lambda)$, the absorption coefficient $a(\lambda)$, the particle-size distribution, the particle concentration, and the chlorophyll a concentration (for the chlorophyll-bearing species). The optical measurements in the selected studies were made from 350 or 400 nm to 750 nm at 1- or 2.5-nm intervals. All final optical quantities are determined at 1-nm intervals from 350 to 750 nm, so appropriate interpolation and/or extrapolation was applied to original data, if necessary.

The single-particle optical cross sections $\sigma_{a,\mathrm{pla},i}(\lambda)$, $\sigma_{b,\mathrm{pla},i}(\lambda)$, and $\sigma_{c,\mathrm{pla},i}(\lambda)$ for the ith planktonic component were calculated from measurements as a ratio of the respective bulk coefficients $a_{\mathrm{pla},i}(\lambda)$, $b_{\mathrm{pla},i}(\lambda)$, and $c_{\mathrm{pla},i}(\lambda)$ to the particle concentration $N_{\mathrm{pla},i}$ [where $b_{\mathrm{pla},i}(\lambda)$ was obtained as a difference, $c_{\mathrm{pla},i}(\lambda) - a_{\mathrm{pla},i}(\lambda)$]. As a result, these cross sections are subject to uncertainties associated solely with measurements. These uncertainties are quantifiable and are generally small. On the other hand, direct measurements of the volume-scattering function over the entire angular range from 0° to 180° with high spectral resolution are currently impossible. The scattering functions were therefore determined from Mie-scattering calculations for homogeneous spheres.[31] These calculations were constrained by measurements. First, the spectral values of the imaginary

Table 1. Summary of Planktonic Components[a]

Label	Planktonic Component	D (μm)	n 550 nm	$n' \times 10^3$ 440 nm	$n' \times 10^3$ 675 nm	$\mathrm{Chl}_{\mathrm{cell}}$ (pg)	Ref.
VIRU	Viruses	0.07	1.050	0	0	0	25
HBAC	Heterotrophic bacteria	0.55	1.055	0.509	0.057	0	24
PROC	Generic *Prochlorophyte*; the average of	0.66	1.051	18.51	10.30	1.466×10^{-3}	
	Prochlorococcus strain MED	0.59	1.055	23.25	13.77	1.433×10^{-3}	27
	average of *Prochlorococcus* strains NATL and SARG	0.70	1.046	13.78	6.687	1.499×10^{-3}	27
SYNE	Generic *Synechococcus*; the average of:	1.05	1.051	5.587	2.930	2.015×10^{-3}	
	Synechococcus strain MAX41 (*Cyanophyceae*)	0.92	1.047	5.415	2.905	1.173×10^{-3}	27
	Synechococcus strain MAX01 (*Cyanophyceae*)	0.94	1.049	4.505	2.547	1.521×10^{-3}	27
	Synechococcus strain ROS04 (*Cyanophyceae*)	1.08	1.049	4.516	2.154	1.260×10^{-3}	27
	Synechococcus strain DC2 (*Cyanophceae*)	1.14	1.050	4.249	2.375	1.495×10^{-3}	27
	Synechococcus strain WH8103 (*Cyanophyceae*)	1.14	1.062	9.251	4.668	4.626×10^{-3}	30
SYMA	Generic phycocyanin-rich picophytoplankton; the average of	1.41	1.055	6.495	2.757	4.497×10^{-3}	
	Synechocystis (*Cyanophyceae*)	1.39	1.050	4.530	1.910	3.644×10^{-3}	26
	Anacystis marina (*Cyanophyceae*)	1.43	1.060	8.460	3.603	5.350×10^{-3}	26
PING	*Pavlova pinguis* (*Haptophyceae*)	3.97	1.046	4.177	2.709	1.198×10^{-1}	23
PSEU	*Thalassiosira pseudonana* (*Bacillariophyceae*)	3.99	1.045	9.231	7.397	3.091×10^{-1}	28
LUTH	*Pavlova lutheri* (*Haptophyceae*)	4.26	1.045	5.767	2.403	1.082×10^{-1}	23
GALB	*Isochrysis galbana* (*Haptophyceae*)	4.45	1.056	7.673	5.101	3.210×10^{-1}	26
HUXL	*Emiliania huxleyi* (*Haptophyceae*)	4.93	1.050	5.012	2.950	2.397×10^{-1}	26
CRUE	*Porphyridium cruentum* (*Rhodophyceae*)	5.22	1.051	3.351	2.443	2.861×10^{-1}	23
FRAG	*Chroomonas fragarioides* (*Cryptophyceae*)	5.57	1.039	4.275	2.904	3.294×10^{-1}	26
PARV	*Prymnesium parvum* (*Haptophyceae*)	6.41	1.045	2.158	1.329	2.889×10^{-1}	23
BIOC	*Dunaliella bioculata* (*Chlorophyceae*)	6.71	1.038	10.49	7.839	2.270	26
TERT	*Dunaliella tertiolecta* (*Chlorophyceae*)	7.59	1.063	6.260	5.076	1.705	29
CURV	*Chaetoceros curvisetum* (*Bacillariophyceae*)	7.73	1.024	2.877	1.480	3.314×10^{-1}	23
ELON	*Hymenomonas elongata* (*Haptophyceae*)	11.77	1.046	13.87	7.591	9.384	26
MICA	*Prorocentrum micans* (*Dinophyceae*)	27.64	1.045	2.466	1.710	25.38	26

[a]Values for the average equivalent spherical diameter D, the real part of the refractive index at 550 nm n, imaginary part of the refractive index at 440 and 675 nm n', and chlorophyll a content per cell $\mathrm{Chl}_{\mathrm{cell}}$ are shown for each component. A taxonomic class of planktonic species is in parentheses. References that provide data are also indicated.

and real parts of the refractive index for each planktonic component, $n'(\lambda)$ and $n(\lambda)$, respectively, were estimated from an inverse model where measurements of spectral beam attenuation, spectral absorption, particle concentration, and size distribution were used.[24,32] Then, the forward Mie calculations of the spectral scattering phase functions $\tilde{\beta}_{\mathrm{pla},i}(\Psi, \lambda)$ were made by using the estimated refractive index and measured particle-size distribution as inputs. Admittedly, there is some unknown degree of uncertainty in the estimated phase functions, primarily because the calculations are based on the assumption of sphericity and homogeneity of planktonic cells. This uncertainty also affects the estimates of backscattering cross sections, $\sigma_{bb,\mathrm{pla},i}(\lambda)$, because the phase function is used first to determine the backscattering ratio $\tilde{b}_{b,\mathrm{pla},i}(\lambda)$, which is a ratio of backscattering to total scattering, and then $\sigma_{bb,\mathrm{pla},i}(\lambda)$ is calculated as a product of $\tilde{b}_{b,\mathrm{pla},i}(\lambda)$ and $\sigma_{b,\mathrm{pla},i}(\lambda)$.

Spectra of absorption, scattering, and backscattering cross sections, as well as a backscattering ratio for 18 planktonic components, are shown in Figs. 1–4. The magnitude and spectral shapes of these optical properties vary dramatically among the components, primarily as a result of the large variation in cell size. For example, the absorption cross sections at different wavelengths span 5–7 orders of magnitude among various planktonic species (Fig. 1). The lowest values are for HBAC and the highest values for (MICA). VIRU are not included in Fig. 1, assuming that these particles have negligible absorption. The scattering cross sections span 8–9 orders of magnitude (Fig. 2) and the backscattering cross sections 6–7 orders of magnitude (Fig. 3). VIRU have the lowest and MICA the highest values for these cross sections. The estimates of backscattering ratio $\tilde{b}_b(\lambda)$ remain below 10^{-2} for all components with the exception of VIRU (Fig. 4). For most phytoplankton components the $\tilde{b}_b(\lambda)$ values are of the order of 10^{-3}. The scattering phase function also shows a large variation among the planktonic components (Fig. 5). Although the phase function for the smallest particles, viruses, shows a relatively weak dependence on the scattering angle, the remaining functions are strongly peaked in the forward direction. The phase functions exhibit some spectral dependence, which is illustrated in Fig. 6 for two selected phytoplankton species differing significantly in cell size.

The optical properties of planktonic microorganisms as well as the methodology of measurements and calculations of these properties are discussed in greater detail in the eight references that provided the original data for this study[23–30] and also more recently in Stramski and Mobley.[33] Nevertheless

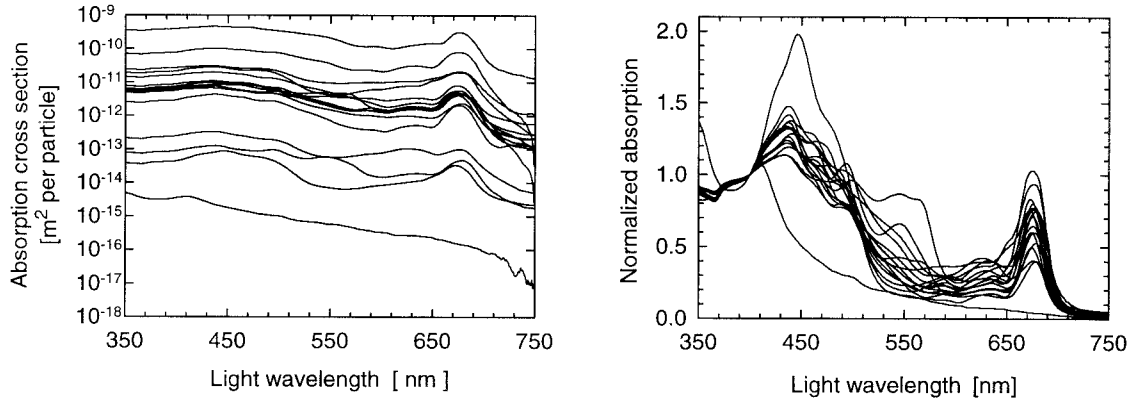

Fig. 1. (Left) Absorption cross sections of the 17 planktonic components VIRU are not included in this graph because their absorption cross sections are assumed to be zero. The lowest curve corresponds to HBAC and the highest curve to MICA. (Right) Each absorption curve is normalized at 400 nm to facilitate comparison of the spectral shapes.

some aspects of that study deserve special attention here.

The data were obtained from measurements of the bulk optical properties of cell suspensions. Typically, thousands of cells were contained within the volume of the culture illuminated for measurements of the beam attenuation and absorption coefficients. Consequently, the single-particle properties represent an average cell (or particle) derived from the investigated population of cells. This average particle is characterized by the optical properties that, after multiplication by the concentration of particles, reproduce the bulk absorption and scattering properties of the actual population of particles. This fea-

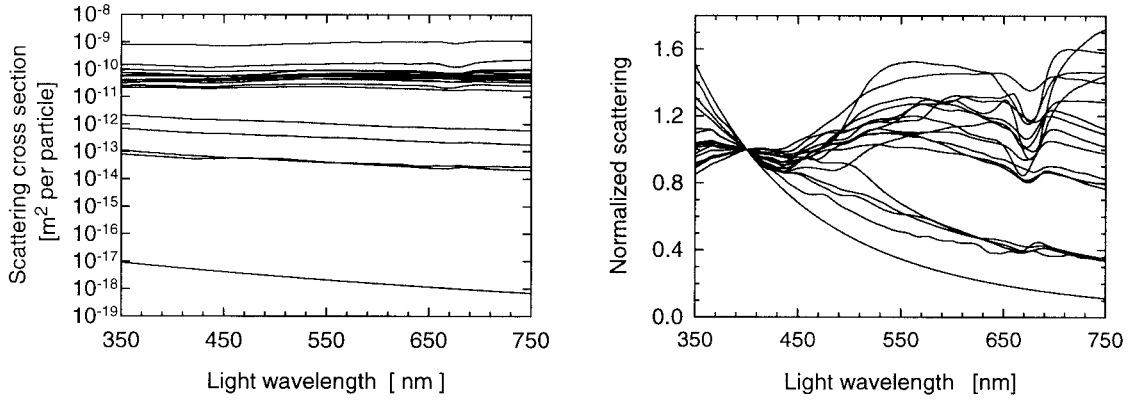

Fig. 2. (Left) Scattering cross sections of the 18 planktonic components. The lowest curve corresponds to VIRU and the highest curve to MICA. (Right) Each scattering curve is normalized at 400 nm to facilitate comparison of the spectral shape.

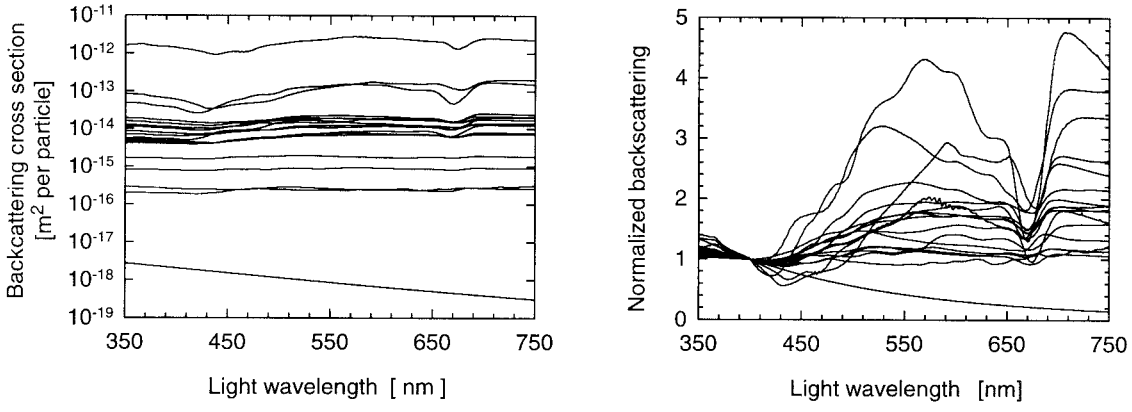

Fig. 3. (Left) Backscattering cross sections of the 18 planktonic components. The lowest curve corresponds to VIRU and the highest curve to MICA. (Right) Each backscattering curve is normalized at 400 nm to facilitate comparison of the spectral shape.

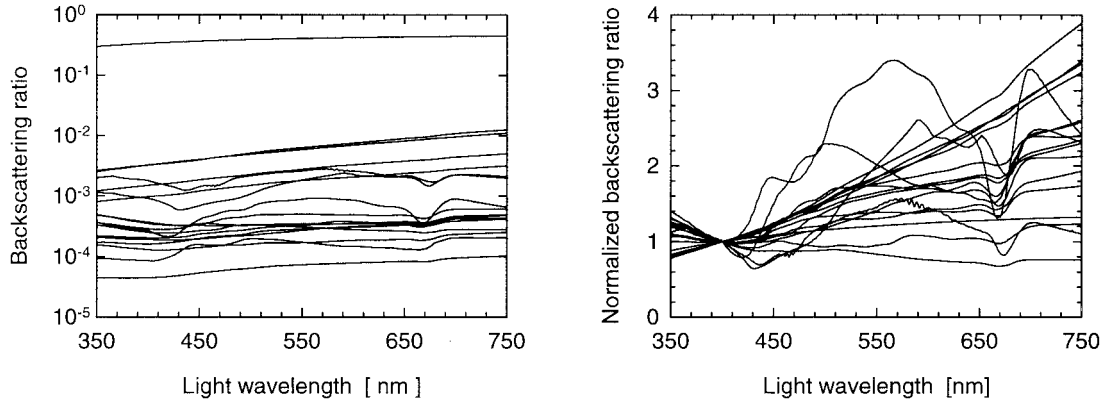

Fig. 4. (Left) Backscattering ratio (i.e., the ratio of backscattering to total scattering) of the 18 planktonic components. The lowest curve corresponds to CURV and the highest curve to VIRU. (Right) Each curve is normalized at 400 nm to facilitate comparison of the spectral shape.

ture is essential to our modeling of the bulk IOPs of a water body as discussed above [see Eqs. (1) and (2)]. An alternative approach to producing data from measurements on individual particles would be impractical because the development of understanding of the bulk optical properties based on each and every particle suspended in natural water bodies is unrealistic. The practical approach must be based on a manageable number of particulate components that realistically represent the mix of optically significant suspended materials. In this regard the characterization of a given particle type in terms of average particle properties derived from a given particulate population is appropriate.

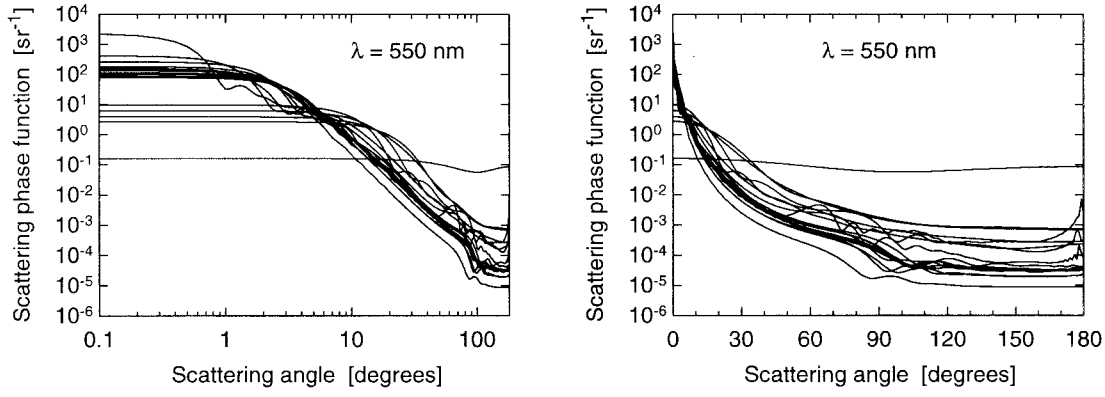

Fig. 5. Scattering phase functions at 550 nm of the 18 planktonic components. (Left) Log–log plot to facilitate comparison of forward-angle scattering. (Right) Semilog plot to facilitate comparison of large-angle scattering including backscattering at angles >90°. The curve that shows a weak dependence on the scattering angle corresponds to VIRU.

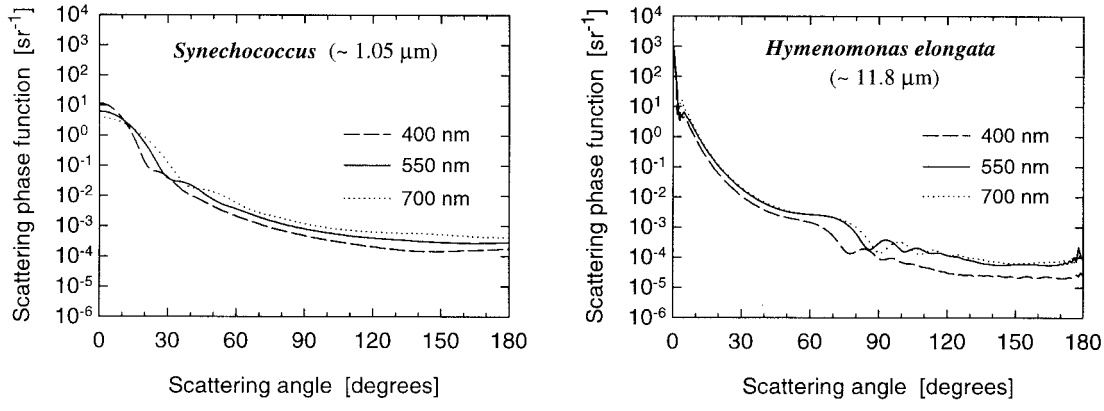

Fig. 6. Scattering phase functions at three different wavelengths, 400, 550, and 700 nm, for two planktonic species: (left) SYN and (right) ELON. The average cell size for these species is indicated.

Naturally the data set that we assembled does not represent every possible detail of the variability in the optical properties of planktonic microorganisms. Our interest here is focused on interspecies variability. This type of variability is important because the average single-particle optical properties vary over many orders of magnitude among various species that range from submicrometer cells to microplanktonic cells being tens of micrometers in size as shown in Figs. 1–5. Note, however, that the average single-particle properties for any particular species could vary in response to changing conditions for growth, for example, irradiance, nutrient availability, or temperature. These variations are referred to as intraspecies variability. A comprehensive description of this type of variability is not possible at the present time because of the lack of optical data for various planktonic species over a broad range of growth conditions. Most species in our data set were examined in a predetermined single set of growth conditions. A few species were examined in varying growth conditions, and in this case the final quantities were obtained by averaging the observed variability (for example, *T. pseudonana* was studied under a diel cycle of irradiance).

4. Optical Properties of Detritus, Mineral Particles, and Bubbles

Both detrital and mineral particles suspended in the ocean are diverse in size, refractive index, and shape and hence in their optical properties. The effect of these particulate components on the bulk optical properties of seawater can range from optically insignificant to optically overwhelming; for example, the presence of suspended minerals may totally dominate some coastal areas affected by river discharge, bottom resuspension, or shore erosion. Similarly, intermittent events of bubble entrainment by breaking waves, especially during high seas, can dominate light scattering at shallow depths,[34] but these effects are still poorly understood. At present it would be impossible to attempt to model detritus and minerals with the same level of detail as microorganisms because of the lack of data and knowledge about the complexity of these particulate components. With regard to detritus and minerals, our objective in this study is merely to use reasonable estimates of the bulk IOP's of these components to provide background in the simulations of the IOP model. Any approach to achieving this objective will necessarily involve some approximations.

With our approach first we calculate the absorption and scattering cross sections and phase functions for an average detrital particle and mineral particle. These average particles represent certain hypothetical populations of particles. This approach is consistent with that for microorganisms in the sense that the bulk optical coefficients can be calculated as a product of the optical cross sections and particle concentration [see Eqs. (1) and (2)]. The estimates of the single-particle properties of detritus and minerals were obtained from Mie-scattering calculations for homogeneous spheres. The approximations to the size distributions and complex index of refraction of detrital and mineral components were used as inputs to these calculations. With these approximations, the components will be referred to as generic detrital (DET) particles and generic mineral (MIN) particles. Because we are ultimately interested in the bulk optical properties of detritus and minerals, whose magnitudes can be easily controlled by varying the particle concentration, the purpose of Mie calculations is merely to provide reasonable estimates of the spectral shapes of the optical cross sections and the relative proportions of absorption and scattering for the DET and MIN components. The magnitudes of our estimates of the single-particle optical properties of DET and MIN should be interpreted with special caution, because the average DET and MIN particles represent hypothetical populations of particles defined by specific assumptions about the refractive index and size distribution that covers a broad range of particle size.

DET was modeled as an assemblage of particles with a wavelength-independent real part of refractive index, $n = 1.04$ (relative to water), diameters ranging from 0.05 to 500 μm and the Junge (differential) size distribution described by a power function with a slope of -4. The spectrum of the imaginary part of refractive index $n'(\lambda)$ was derived from the microspectrophotometric data of individual detrital particles of Iturriaga and Siegel[35] by using a method described by Bricaud and Morel.[32] Specifically, in this derivation we used the Iturriaga and Siegel estimates of the mean spectral absorption efficiency factors and the mean cross-sectional area of detrital particles sampled at nine depths between 4 and 107 m at two stations in the Sargasso Sea. Iturriaga and Siegel took measurements of 11–35 individual particles at each depth, and the total number of particles examined was 176. The mean equivalent diameter of these particles varied from $\sim$9 to 27 μm among the depths. We first calculated $n'(\lambda)$ at each depth separately and then averaged these results to obtain the final spectrum $n'(\lambda)$. Because the microspectrophotometric data were available only at ten wavelengths between 410 and 675 nm, our calculations included fitting the exponential function to these data, so that $n'(\lambda)$ could be determined from 350 to 750 nm at 1-nm intervals. The final spectrum of $n'(\lambda)$ for DET is described as $n'(\lambda) = 0.0010658 \exp(-0.007186\lambda)$. This exponential function is consistent with previous observations of the detrital absorption coefficient in the ocean.[14–16]

For mineral particles we assumed the same size distribution and $n'(\lambda)$ values as for organic detritus. Relatively few data on $n'(\lambda)$ of minerals are available for the visible spectrum.[36,37] For common clay minerals such as kaolinite and montmorillonite the reported n' values are generally of the order of 10^{-4}, which is similar to our estimates for DET. Note, however, that other mineral species could show lower (for example, quartz and calcite) or higher (hematite) values of $n'(\lambda)$ at visible wavelengths.[37] The real

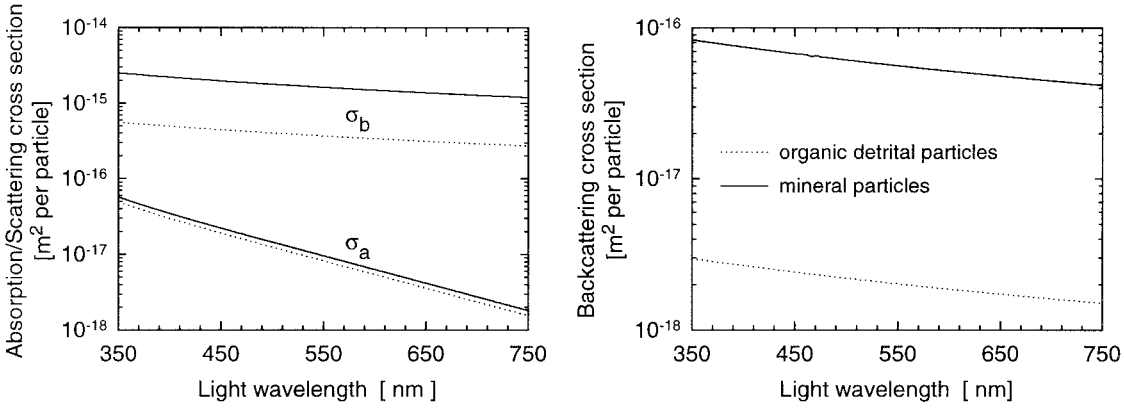

Fig. 7. (Left) Absorption σ_a and scattering σ_b cross sections for generic assemblages of organic detrital particles (dotted lines) and mineral particles (solid lines). (Right) Backscattering cross sections of these two components.

part of the refractive index of minerals was taken to be 1.18 at all wavelengths, which is also a reasonable choice as a first approximation.[38,39] Accordingly, although MIN represents high-index inorganic particles, DET can be thought of as a component representing low-index organic particles (primarily nonliving particles but also possibly heterotrophic organisms not included in the present description of the planktonic community).

The assumptions involved in the estimation of the optical properties of DET and MIN are acceptable in this study for the following reasons. Currently, it would be impossible, and we do not intend to model the exact distributions of particle size and refractive index of detrital and mineral particles. It is known that any simple function, such as a power-law function, cannot accurately describe details of the actual particle-size distributions at a fine size resolution,[40] because these distributions exhibit various features and variations in slope over different portions of the size spectrum, which are difficult to predict.

Nevertheless, to a first approximation, a power function with a single slope can describe the most prominent feature at a large-size scale, which is a decrease of particle concentration with increasing particle size from the submicrometer range to hundreds of micrometers. In this approximation the value of -4 is a reasonable choice for the slope of the distribution, although in reality the slope varies in the ocean with environmental conditions and also with the particle size within any given distribution. Most important, by using the -4 power law and the approximate values of the refractive index, we estimated the spectral shapes of the optical cross sections and the relative proportions of absorption and scattering with a reasonable approximation. By using these cross sections and choosing appropriate particle concentrations in the simulations of the IOP model as described below, we can calculate the desired bulk optical coefficients of the entire populations of detrital and mineral particles [Eqs. (1) and (2)], which are consistent with the available information from field studies. We emphasize that this approach can be viewed only as a first-order approximation for estimating background contributions of detritus and minerals in our IOP model, which is currently focused on the planktonic community.

Similar rationale and approximations apply to the generic bubble (bub) component. We assumed that air bubbles range in diameter from 20 to 500 μm and that their real part of refractive index relative to water is 1.34^{-1}. The imaginary part was assumed to be zero. The size distribution was derived from acoustic measurements of bubbles made at a wind speed of $\sim$11 ms^{-1}.[41] Specifically, we obtained the final size distribution by averaging the distributions determined by Vagle and Farmer at four depths, 1.1, 2.7, 4.9, and 7.3 m, each representing a 5-min time average. Because these determinations were limited to diameters smaller than 260 μm, we used an extrapolation to 500 μm. The difference between the spectral scattering cross sections of the average bubble derived from the final size distribution and the corresponding cross sections derived from the actual distributions measured at the four depths varies from -10% to 12%. A similar comparison for the spectral scattering phase functions $\tilde{\beta}_{\mathrm{bub}}(\Psi, \lambda)$ shows that these differences are within $\pm 10\%$ if a comparison is made for scattering angles Ψ between 1° and 179°. We emphasize, however, that the bubble size distributions could in reality show considerable variations with time and depth.

Figure 7 shows absorption, scattering, and backscattering cross sections for detritus and minerals. These cross sections are smooth monotonic functions of λ. Table 2 shows the best-fit equations describing these spectra. The slope of the exponential function describing $\sigma_{a,\mathrm{DET}}(\lambda)$ and $\sigma_{a,\mathrm{MIN}}(\lambda)$ is approximately -0.0085, which is within the range of values (-0.0024 to -0.017) reported for the detrital absorption coefficient measured on oceanic particle assemblages.[15,16] The exponent of the power function describing the scattering cross sections $\sigma_{b,\mathrm{DET}}(\lambda)$ and $\sigma_{b,\mathrm{MIN}}(\lambda)$ is close to -1, which is consistent with the scattering coefficient by particles that obey the Junge size distribution with a slope of -4.[4] The backscattering spectra, $\sigma_{bb,\mathrm{DET}}(\lambda)$ and $\sigma_{bb,\mathrm{MIN}}(\lambda)$, are somewhat less steep than the total scattering spectra, with

Table 2. Spectral Absorption σ_a, Scattering σ_b, and Backscattering σ_{bb} Cross Sections for the Generic Components of Detrital Particles, Mineral Particles, and Air Bubbles[a]

Component	Absorption	Scattering	Backscattering
Detritus	$\sigma_{a,\mathrm{det}}(\lambda) = 8.791 \times 10^{-4} \times \exp(-0.00847\lambda)$	$\sigma_{b,\mathrm{det}}(\lambda) = 0.1425\lambda^{-0.9445}$	$\sigma_{bb,\mathrm{det}}(\lambda) = 5.881 \times 10^{-4}\,\lambda^{-0.8997}$
Minerals	$\sigma_{a,\mathrm{min}}(\lambda) = 1.013 \times 10^{-3} \times \exp(-0.00846\lambda)$	$\sigma_{b,\mathrm{min}}(\lambda) = 0.7712\lambda^{-0.9764}$	$\sigma_{bb,\mathrm{min}}(\lambda) = 1.790 \times 10^{-2}\,\lambda^{-0.9140}$
Bubbles	$\sigma_{a,\mathrm{bub}}(\lambda) = 0$	$\sigma_{b,\mathrm{bub}}(\lambda) = 4607.873\ (\pm 5.555)$	$\sigma_{bb,\mathrm{bub}}(\lambda) = 55.359\ (\pm 0.373)$

[a]Best-fit equations for detrital and mineral components are shown. The squared correlation coefficients for these relationships (as calculated after appropriate logarithmic transformation of variables) are greater than 0.999. The scattering of the bubble component is nearly independent of λ, so the average values and standard deviations (in parentheses) based on all spectral values between 350 and 750 nm are given. The cross sections are in units of μm^2, and λ is in nanometers. We caution against indiscriminate use of the magnitudes of these cross sections (see text for details).

the corresponding exponent being approximately -0.9. Finally, scattering and backscattering for air bubbles are nearly independent of λ, so that the spectrally averaged values provide a good approximation to $\sigma_{b,\mathrm{bub}}(\lambda)$ and $\sigma_{bb,\mathrm{bub}}(\lambda)$ (Table 2).

The scattering phase functions for DET, MIN, and bub at $\lambda = 550$ nm are compared with the average particle-phase function based on Petzold's measurements[10] in Fig. 8. Significant differences are observed among the functions. The mineral particles show relatively less scattering at small angles and more scattering at large angles compared with other components and Petzold's curve, which primarily results from the high refractive index of minerals. For very small angles, $\Psi < 1°$, $\tilde{\beta}_{\mathrm{bub}}(\Psi, \lambda)$ of bubbles has the steepest slope, and it also displays a pronounced minimum within the range of backscattering angles, $\Psi > 90°$. The phase function for low-index detrital particles shows the least backscattering among the compared curves. Variations in $\tilde{\beta}(\Psi, \lambda)$ with λ are generally small (not shown here). For example, for detritus and minerals the values for $\tilde{\beta}(\Psi, 400)$ and $\tilde{\beta}(\Psi, 700)$ differ from $\tilde{\beta}(\Psi, 550)$ at various Ψ by no more than a few percent. Only for Ψ near 180° these differences could exceed 10%. For bubbles the spectral differences remain within a few percent for $\Psi > 10°$ and exceed 20% for $\Psi < 2.5°$.

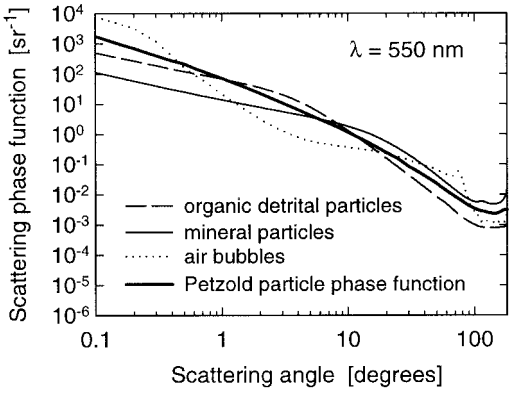

Fig. 8. Comparison of scattering phase functions (at 550 nm) of detrital particles, mineral particles, air bubbles, and the average Petzold particle phase function. The Petzold phase function is taken from Mobley (Table 3.10, p. 111).[10]

5. Example Simulations of the Inherent Optical Property Model

We now discuss example simulations of the IOP model. Because our interest is focused on the optical effects of the detailed composition of the planktonic community, pure water and dissolved organic matter are not considered. Thus the simulations of the model include 20 components that absorb light [see Eq. (1)] and 21 components that scatter light [see Eq. (2)]. Equations (1) and (2) indicate that, to model the total IOP's in terms of component contributions, we must specify the optical properties on a per particle basis and particle concentrations of each component in a water body. The optical properties on a per particle basis are described above, so it remains to specify the concentrations.

A. Base Simulation of Oligotrophic Waters

In Table 3 we show the concentrations assumed for the 21 components involved in the simulation, which will be referred to as the base set of concentrations or base simulation. Although it is not our purpose to reproduce exactly the detailed composition of any particular water body within the ocean, the base simulation can represent the IOPs of relatively clear oligotrophic water with considerable realism. The total concentration of chlorophyll *a* in this simulation is ~ 0.18 mg m^{-3}. In addition to microorganisms and organic detritus, the simulated water body contains some mineral particles and bubbles.

The corresponding particle-size distributions are shown in Fig. 9. The concentrations of all planktonic components including viruses were chosen to represent realistic values encountered in natural waters.[42–48] For example, flow cytometry measurements by Li[48] showed that the abundance of *Prochlorococcus* in the central North Atlantic Ocean within the top 200 m varies from $\sim 10^7$ to 2×10^{11} cells m^{-3}. In that study the mean contribution of *Prochlorococcus* to the total number of ultraphytoplankton cells with a diameter smaller than ~ 5 μm was 78%. In our base simulation the PROC concentration of 1.75×10^{10} cells m^{-3} is close to the mean value measured by Li[48] in surface waters from May to June 1993. PROC contributes nearly 71% to the total concentration of phytoplankton cells (all components

Table 3. Particle Number and Chlorophyll *a* Concentrations of Various Particulate Components Used in the Base Simulation of the IOP Model[a]

Component	Concentration (particles/m^3)	Chl *a* (mg m^{-3})
VIRU	2.5×10^{12}	0
HBAC	1.0×10^{11}	0
PROC	1.75×10^{10}	2.5654×10^{-2}
SYNE	5.0×10^{9}	1.0076×10^{-2}
SYMA	2.0×10^{9}	8.9940×10^{-3}
PING	1.1264×10^{8}	1.3499×10^{-2}
PSEU	2.4520×10^{7}	7.5798×10^{-3}
LUTH	2.4809×10^{7}	2.6852×10^{-3}
GALB	1.2097×10^{7}	3.8830×10^{-3}
HUXL	1.0848×10^{7}	2.6001×10^{-3}
CRUE	1.1240×10^{7}	3.2161×10^{-3}
FRAG	1.1920×10^{7}	3.9260×10^{-3}
PARV	1.5619×10^{7}	4.5122×10^{-3}
BIOC	0.9915×10^{7}	2.2511×10^{-2}
TERT	0.8925×10^{7}	1.5217×10^{-2}
CURV	0.7467×10^{7}	2.4745×10^{-3}
ELON	4.25×10^{6}	3.9883×10^{-2}
MICA	5.0×10^{5}	1.2692×10^{-2}
DET	8.25×10^{13}	0
MIN	2.75×10^{13}	0
BUB	1.775×10^{6}	0
Picoplankton	1.245×10^{11}	4.4724×10^{-2}
Small nanoplankton	2.5×10^{8}	8.2104×10^{-2}
Total plankton	2.6248×10^{12}	0.1794
Total nonliving particles	1.1×10^{14}	0

[a]Picoplankton is the sum of HBAC, PROC, SYNE, and SYMA, Small nanoplankton is the sum of 11 phytoplankton components from PING through CURV, and Total plankton includes all 18 planktonic components from VIRU through MICA. Total nonliving particles represent the sum of DET and MIN, and BUB indicates the air bubble component.

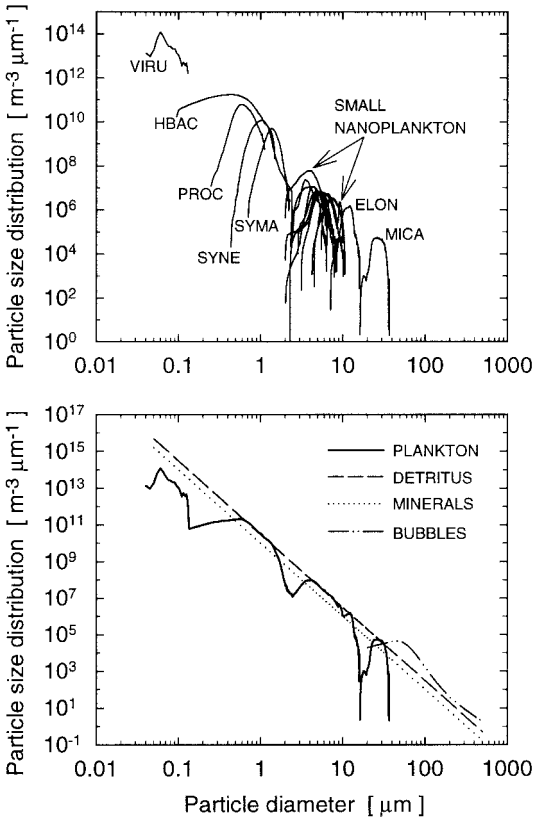

Fig. 9. (Top) Density functions of the particle-size distribution for the 18 planktonic components at the base concentrations shown in Table 3. The 11 distributions for small nanoplankton species are indicated by arrows. (Bottom) Composite size distribution of all planktonic components, as derived from individual distributions (top) compared with the size distributions of detrital particles, mineral particles, and air bubbles at the concentrations shown in Table 3.

from PROC through MICA) in the simulation, which is also consistent with the Li data.

Another important point is that the planktonic concentrations in Table 3 were defined subject to the constraint that the overall size distribution of the planktonic components (with the exception of viruses) obeys a power law with an exponent of -4 in the size regions where data are available. In other words, if $N_{\mathrm{pla}}(D)\mathrm{d}D$ is the number of all planktonic particles per unit volume in the diameter interval from D to $D + \mathrm{d}D$, the density function of the composite particle-size distribution of plankton $N_{\mathrm{pla}}(D)$ varies as D^{-4}. This is consistent with the assumed size distributions of detritus and minerals, which also vary as D^{-4} (Fig. 9). The gaps in the planktonic data between 1.5 and 4 μm and $D > 10$ μm result in the local decrease in the concentration of planktonic cells to levels below what would be expected from the -4 law. The concentration of planktonic cells finally declines to zero at $D > 40$ μm.

The particle concentration for DET was chosen to yield the absorption coefficient of DET at 440 nm $a_{\mathrm{DET}}(440)$ of ~20% of the total particulate absorption, $a_p(440)$. The selected concentration of minerals provides a contribution of ~8% to $a_p(440)$. As a result the overall contribution of nonliving particles (DET + MIN) to $a_p(440)$ in the base simulation is ~29%. The above numbers are consistent with the range of values representing absorption by nonliving particles observed in the ocean at a similar Chl.[16] As for the magnitudes of the optical cross sections of DET and MIN, we caution against attaching particular significance to the selected concentrations of DET and MIN in the context of how well these values can represent realistic concentrations in the ocean. With regard to the DET and MIN components, the most important aspect of our IOP model is a choice of the realistic contributions of a_{DET} and a_{MIN} to a_p, which are determined by the product of the absorption cross sections and particle concentrations. The concentration of air bubbles was selected to be consistent with measurements by Vagle and Farmer[41] at depths between 2 and 3 m and a wind speed of 11 ms^{-1}.

In addition to particle concentrations, Table 3 also shows how chlorophyll *a* is distributed among various phytoplankton components in the base simulation. The small nanoplankton species covering the size range from ~4 to 8 μm (components PING through CURV in Table 1 together) make the major contribu-

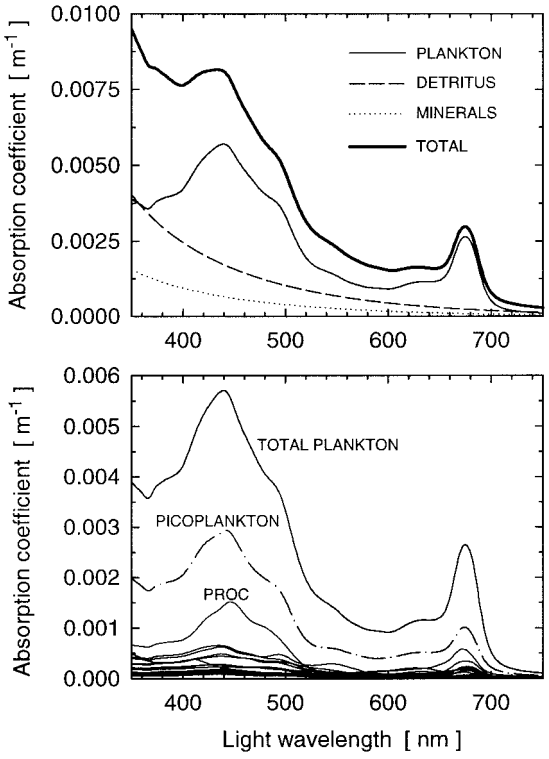

Fig. 10. (Top) Total absorption coefficient by suspended particulate matter and the contributions associated with all planktonic components, detritus, and mineral particles as obtained from the base simulation of the IOP model. (Bottom) Absorption coefficient of plankton further partitioned into the contributions associated with the various planktonic components. The single most important planktonic component is PROC, and the most dominant planktonic group is picoplankton.

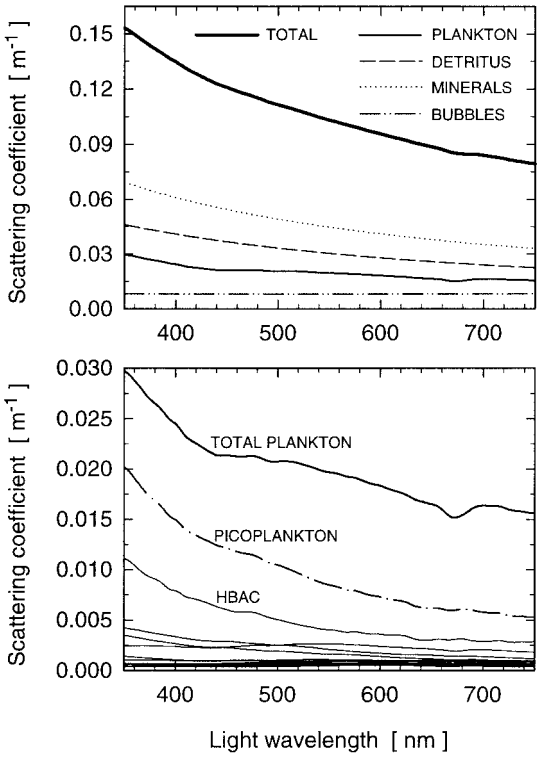

Fig. 11. (Top) Total scattering coefficient by suspended hydrosols and the contributions associated with all planktonic components, detritus, mineral particles, and air bubbles as obtained from the base simulation of the IOP model. (Bottom) Scattering coefficient of plankton further partitioned into the contributions associated with the various planktonic components. The single most important planktonic component is HBAC, and the most dominant planktonic group is picoplankton.

tion of 45.8% to total Chl. The picophytoplankton components (PROC, SYNE, and SYMA) contribute 24.9%, and two larger species, ELON and MICA, contribute 29.3% to Chl.

The spectra of absorption, scattering, and backscattering coefficients obtained from the base simulation are shown in Figs. 10–12. These plots illustrate how our approach provides a detailed understanding of the effects of various planktonic components on the bulk IOPs. In the simulated water the total absorption coefficient by all particulate components $a_p(\lambda)$ is dominated by planktonic absorption $a_{\mathrm{pla}}(\lambda)$ for most wavelengths between 400 and 700 nm (Fig. 10). This is a direct consequence of our choice of the realistic contributions of nonliving particles to $a_p(\lambda)$ as described above. Note that DET and MIN play an increasingly greater role with decreasing wavelength, which is associated with the exponential shape of their absorption curves. Among the planktonic components the single most important component is PROC, especially within the blue and the red absorption maxima. This result can represent a typical situation in the oligotrophic ocean when the *Prochlorococcus* abundance is sufficiently high, for example, in the central North Atlantic.[48] The dominant contribution of PROC to absorption is remarkable given that this species contributes only 14.3% to the total Chl. The picoplankton components together, PROC, SYNE, SYMA, and HBAC, contribute generally 40–50% to $a_{\mathrm{pla}}(\lambda)$, although chlorophyll a associated with these species constitutes ~25% of the total Chl. Interestingly, nonpigmented HBAC make a noteworthy contribution to $a_{\mathrm{pla}}(\lambda)$ at short wavelengths, for example, 8% at 400 nm. The effect of these bacteria then decreases with wavelength.

A similar analysis for the scattering coefficient shows that the mineral particles are the most important component in our simulation (Fig. 11). The contribution of MIN to the total hydrosol (particles and bubbles) scattering $b_p(\lambda)$ varies between 41% and 45% at different wavelengths. DET is the second most important component with a contribution of ~30%, so even if no minerals were present in the simulated water body the nonliving particles would still dominate scattering. All the planktonic components contribute only 17–20% to $b_p(\lambda)$. Finally, the least important, although not negligible, contribution ranging from 5% at 350 nm to 10% in the red comes from bubbles. Note, however, that at sufficiently strong winds the bubble contribution to scattering near the surface can vary strongly on short time scales owing to the intermittent nature of bubble en-

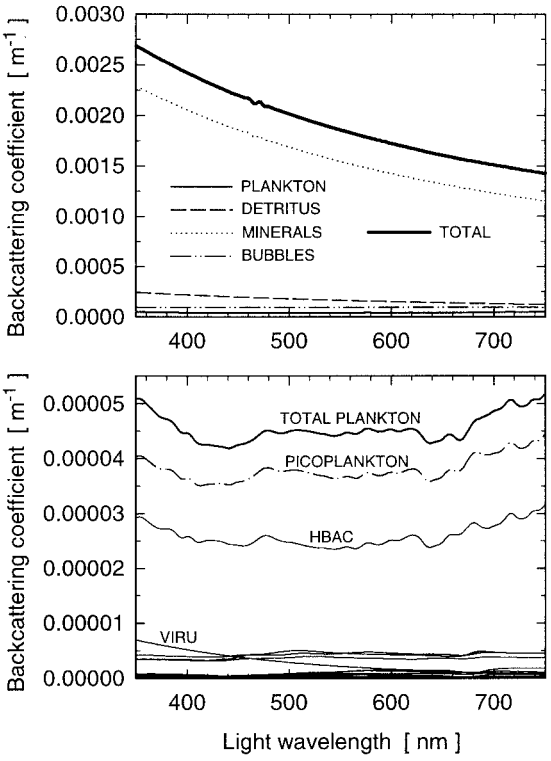

Fig. 12. (Top) Total backscattering coefficient by suspended hydrosols and the contributions associated with all planktonic components, detritus, mineral particles, and air bubbles as obtained from the base simulation of the IOP model. (Bottom) Backscattering coefficient of plankton further partitioned into the contributions associated with the various planktonic components. The single most dominant planktonic component is HBAC, and the most dominant planktonic group is picoplankton. The contribution by VIRU is also highlighted.

trainment by breaking waves.[34] Figure 11 also shows that the single most important scattering component among plankton is HBAC. The contribution of all picoplankton species to total plankton scattering decreases with λ from ~61% at 400 nm to 35% at 700 nm. Viruses make a negligible contribution of less than 1%.

The magnitudes of $a_p(\lambda)$ and $b_p(\lambda)$ indicate that the beam attenuation coefficient by all hydrosols $c_p(\lambda)$ is dominated by the scattering process. The single-scattering albedo, $\omega_{0,p}(\lambda) = b_p(\lambda)/c_p(\lambda)$, ranges from 0.938 at 438 nm to nearly 1 at 750 nm (not shown here). DET and MIN have very high values of $\omega_0(\lambda)$, for example, $\omega_{0,\mathrm{min}}(\lambda)$ increases from 0.978 at 350 nm to almost 1 at 750 nm. The $\omega_{0,\mathrm{BUB}}(\lambda)$ for bubbles is naturally 1 because this is a nonabsorbing component. The planktonic components have generally lower values of ω_0, for example, $\omega_{0,\mathrm{pla}}(\lambda)$ for all the planktonic components combined attains a minimum value of 0.79 in the blue absorption band of chlorophyll a.

The mineral particles are by far the most important backscattering component in the simulated water body (Fig. 12). The contribution of MIN to the total backscattering coefficient by hydrosols $b_{b,p}(\lambda)$ ranges from 80% to 85% across the spectrum. DET contributes ~9%, BUB from 3.6% to 7%, and all the planktonic microorganisms only 1.8–3.6%. BAC backscatter much more light than any other planktonic component, and picoplankton components altogether contribute more than 80% to the planktonic backscattering. The only remarkable role that viruses play in our simulation is the appreciable contribution to planktonic backscattering at short wavelengths, for example, nearly 12% at 400 nm. Nevertheless, as indicated above, the microorganisms altogether have little importance to backscattering in this simulation.

Our model similarly permits a detailed analysis of the volume-scattering function in terms of the component contributions. Here we report only the values for the backscattering ratio, $\tilde{b}_b(\lambda) = b_b(\lambda)/b(\lambda)$, that depend on the shape of the scattering function. For all the planktonic components together this ratio (in percent) increases from 0.18% at 400 nm to 0.3% at 700 nm. For other components the $\tilde{b}_b(\lambda)$ ratio is weakly dependent on λ, being ~0.5% for DET, 3% for MIN, and 1.2% for BUB. The total backscattering ratio for all hydrosols in the simulated water body is ~1.8% at all wavelengths.

B. Species Composition of Small Nanoplankton

The number of planktonic components used in the present IOP model is relatively large. It is therefore of interest to address the question of whether this number could be reduced to simplify the model without adversely affecting the most meaningful predictions of the model. Of the 18 planktonic components in the present data set, 11 phytoplankton species referred to as small nanoplankton (PING through CURV in Table 1) represent the most reasonable choice for this analysis. Although these species can have considerably different optical cross sections, they cover a relatively narrow range in particle size (the average cell size varies from ~4 to 8 μm), and they all play similar roles in the marine environment.

In Table 3 we show just one possible set of concentrations of PING through CURV that satisfies the -4 power law given that the total concentration of these 11 nanoplankton species is 2.5×10^8 m^{-3}. To examine the extent to which the IOPs vary in response to changes in the detailed composition of small nanoplankton, we defined 21 additional sets of concentrations of these 11 species. Each set is still subject to the constraint of the -4 power law for the size distribution. The total concentration of the 11 species in each set remains the same, 2.5×10^8 m^{-3}. When defining these sets, we focused our effort on generating as much variability as possible in the relative contributions of individual species to this total concentration. We tolerated small variations in the slope of the composite size distribution of small nanoplankton around the value of -4. The average slope based on 22 composite distributions (base set plus 21 new sets) as determined across the size range from 4.3 to 8 μm is -3.957. (The standard deviation is 0.056.)

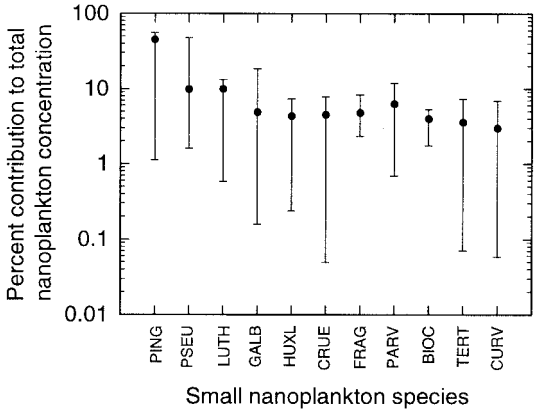

Fig. 13. Range of concentrations for each of the 11 small nanoplankton species from PING through CURV, which represents 22 different sets of nanoplankton composition. The concentrations are shown in terms of their percent contribution to the total nanoplankton concentration, which is 2.5×10^8 particles m^{-3} in the base simulation of the IOP model. The points correspond to the particular set of base concentrations shown in Table 3.

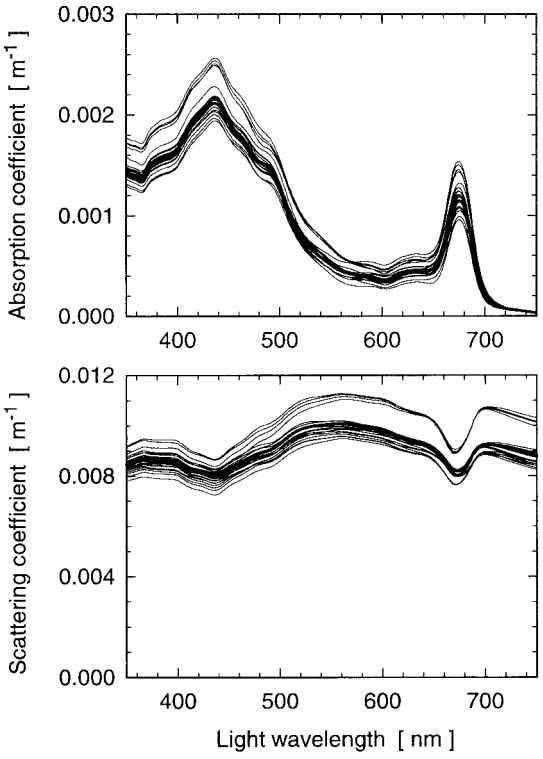

Fig. 14. (Top) Variations in the absorption and (bottom) scattering coefficients of the 11 small nanoplankton species together (i.e., 11 species from PING through CUR) caused by changes in the species composition. Twenty-two absorption and scattering curves are shown that correspond to the 22 different sets of species concentrations. The total concentration of the 11 species combined is the same for each of these 22 sets, that is, 2.5×10^8 particles m^{-3}.

Figure 13 shows that the concentration of each species varies significantly among the 22 sets that we have now defined. The concentrations of FRAG and BIOC change by more than a factor of 3. The variation for other species spans 1–2 orders of magnitude. For example, the contribution of PING to the total concentration of the 11 species varies from 1.1% to 55%, that is, 50-fold. For GALB, CRUE, TERT, and CURV this variation is more than 100-fold. Thus these 22 sets are adequate for examining the effect of the composition of small nanoplankton on IOPs.

Figure 14 shows 22 spectra of absorption and scattering coefficients, $a_{nan}(\lambda)$ and $b_{nan}(\lambda)$. Each spectrum represents the combined effect of the 11 nanoplankton species and corresponds to one of the 22 sets of species concentrations. The $a_{nan}(\lambda)$ and $b_{nan}(\lambda)$ spectra plotted as heavy curves represent the base set of concentrations used in the model simulation discussed above. These heavy-line spectra are similar to the average spectra based on all 22 curves; the differences are within 7% for the spectral absorption values (if λ near 750 nm is ignored) and 2% for the scattering values. In the blue band of chlorophyll *a* at 440 nm the absorption values from individual spectra generally differ by less than 8% from the average value based on all 22 absorption spectra. This difference is greater than 10% for 6 out of 22 curves, reaching 17.7% for one spectrum that differs the most from the average spectrum. For the scattering coefficient at 440 nm, this difference is typically <4% and extends to 9% in the extreme case.

If we used any of the 21 new sets of nanoplankton species composition instead of the base set defined in Table 3, the total IOPs associated with all particulate components and major conclusions from the base simulation would be similar. For example, we compared the total particulate-scattering coefficient from the base simulation shown in Fig. 11 with the values for the 21 remaining sets of nanoplankton composition and found that the differences do not exceed 2%. For the absorption coefficient these differences are generally also within a few percent, although deviations from the base simulation as high as 10–14% occur within a narrow spectral band near 660 nm if the four outlying nanoplankton spectra from Fig. 14 are used. These results suggest that the 11 species from PING through CURV could be treated in our model as a single component if we had no interest in studying the detailed effects of individual species in the size range from ~4 to 8 μm. This would reduce the number of effective planktonic components from 18 to 8 while still allowing one to derive meaningful information from the model simulations. Appropriate values for the optical cross sections and phase functions characterizing the average cell derived from the entire particulate assemblage of the 11 nanoplankton species would have to be used. For example, the absorption and the scattering cross sections of such single nanoplankton component could be determined from the average spectra based on the curves shown in Fig. 14 and the total concentration of the 11 species.

We emphasize that these conclusions are based on the analysis of the particle-size distribution that satisfies the −4 power law. Making such a single-

Table 4. Cell and Chlorophyll-a Concentrations of Bloom-Forming Phytoplankton Species Used in the Model Simulations of Blooms[a]

Bloom-Forming Component	Concentration (cells/m^3)	Chl a (mg m^{-3})
PROC (Prochlorophytes)	3.85×10^{11}	0.5644
SYNE (Cyanobacteria)	2.725×10^{11}	0.5491
PING (Small flagellates)	3.8636×10^{9}	0.5551
LUTH	8.5096×10^{8}	
PSEU (Small diatoms)	1.7679×10^{9}	0.5465
BIOC (Medium-sized green algae)	1.5150×10^{8}	0.5765
TERT	1.3637×10^{8}	
ELON (Relatively large flagellates)	6.1668×10^{7}	0.5787
MICA (Large dinoflagellates)	2.1725×10^{7}	0.5515

[a]Note that five blooms are produced by a single species. In the two remaining cases, two species of similar cell size from the same taxonomic class are grouped together to produce a bloom. The total chlorophyll a concentration in the simulation of each bloom is $\sim$0.718 mg m^{-3}.

component description of small nanoplankton may also be justified when the contributions of these species to absorption and scattering are smaller than those corresponding to the -4 power law. In other cases, however, it may be necessary to consider the detailed composition of small nanoplankton, for example, when various species form blooms (see Subsection 5.C). Nevertheless the results from the above analysis are important because they indicate that certain individual species can be combined (at least in some situations) without adversely affecting the realism of the IOP model. This suggests the possibility of modeling IOPs in terms of the detailed composition of a water body by using a manageable number of effective components, even if more optical data characterizing various particulate components become available in the future.

C. Blooms of Various Phytoplankton Species

The model simulations referred to as blooms of phytoplankton species were devised to demonstrate variations in IOPs that could result from changes in the species composition at the same total chlorophyll a concentration. We made seven simulations of blooms, each of which was produced by one or two dominant species as shown in Table 4. In cases in which two species were chosen to produce a bloom, these species are similar in cell size and belong to the same taxonomic group. For each bloom simulation the total Chl is $\sim$0.718 mg m^{-3}, which is four times higher than that in our base simulation of oligotrophic water. Although the simulations with Chl = 0.718 mg m^{-3} are referred to here as blooms, note that phytoplankton blooms in the ocean can often be characterized by higher chlorophyll concentrations. In the bloom simulations all the components of our model (including DET, MIN, and BUB) with the exception of bloom-forming species are present at the base concentrations given in Table 3. The bloom-forming species are present at cell concentrations (see Table 4) that are higher than those used in the base simulation. The chlorophyll a concentrations associated with the bloom-forming species for each bloom are also shown in Table 4, which indicates that these species contribute 76–80% to the total Chl. The size distributions of planktonic organisms exhibit characteristic features associated with bloom-forming species as shown for the examples representing the blooms of SYNE and ELON (Fig. 15).

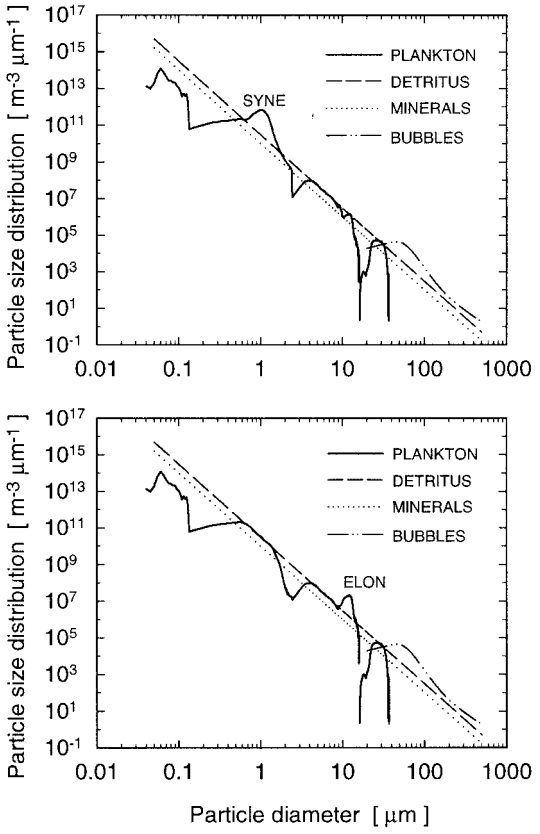

Fig. 15. Examples of particle-size distributions for two bloom simulations of the IOP model, the bloom of SYNE, and the bloom of ELON. The features associated with the bloom-forming species are seen in the size distributions of plankton.

The effects of blooms on the total particulate absorption $a_p(\lambda)$ and scattering $b_p(\lambda)$ coefficients are illustrated in Fig. 16. There is a large variation (as much as four-fold at some wavelengths) in the $a_p(\lambda)$ values among the blooms. The blue and red spectral regions show a clear pattern; the highest values of $a_p(\lambda)$ are observed for the blooms of picophytoplankton, PROC and SYNE, and the relatively low values for the blooms of larger species, BIOC and TERT, ELON, and MICA. We do not suggest, however, that $a_p(\lambda)$ shows a regular decrease with the increasing cell size of the bloom-forming species. Note also that even the blooms of larger species produce $a_p(\lambda)$ values that are significantly higher than those for the base simulation of the oligotrophic ocean. These results demonstrate that changes in the species com-

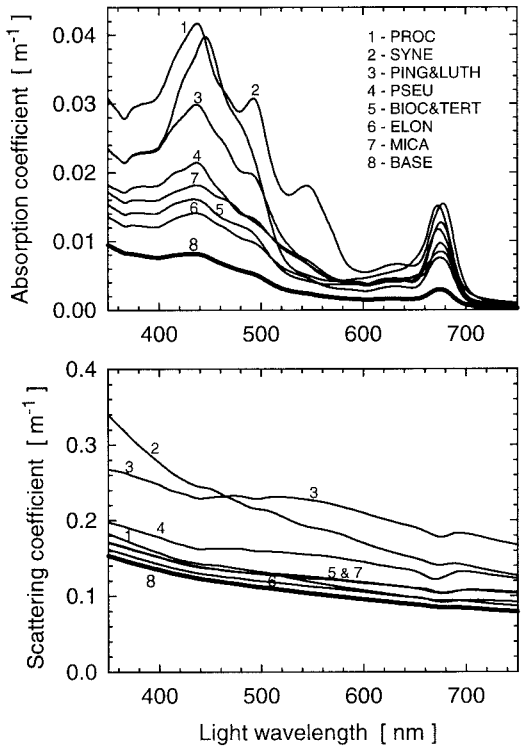

Fig. 16. (Top) Spectra of the total particulate absorption coefficient and (bottom) total particulate scattering coefficient obtained from the bloom simulations of the IOP model. Labels 1–7 correspond to various blooms as indicated. For comparison, the spectra from the base simulation of the oligotrophic water are also shown. (The lowest curve in each figure is shown as a thick solid curve).

position can induce large variations in the particulate absorption although the total chlorophyll concentration remains unchanged. Obviously, this also indicates a similar variability in the chlorophyll-specific absorption coefficient associated with changes in the species composition.

The various blooms also produce a significant variation in the scattering coefficient $b_p(\lambda)$. The extent of this variation is somewhat smaller than that for $a_p(\lambda)$, and there is no consistent effect of the cell size of bloom-forming species on the magnitude of $b_p(\lambda)$. At most wavelengths the highest values of $b_p(\lambda)$ are observed in the bloom of small flagellates, PING and LUTH. At the short-wavelength end of the spectrum, the bloom of cyanobacteria SYNE produces the most scattering. Some blooms result in a relatively small enhancement of $b_p(\lambda)$ compared with the values obtained in the base simulation of oligotrophic water. For the ELON bloom, this enhancement is only 5–15% although Chl increased fourfold between the base simulation and the ELON bloom. Regarding the particulate backscattering coefficient $b_{bp}(\lambda)$, there is little variability among the blooms (not shown here). In addition, most of the examined blooms induce a very small increase (3% or less) in $b_{bp}(\lambda)$ compared with the values from the base simulation. In the case of the SYNE bloom when $b_{bp}(\lambda)$ is highest among all the simulations, this enhancement in the red part of the spectrum is ~15%.

6. Conclusions

We have presented a reductionist approach to modeling the ocean's inherent optical properties based on the data of various planktonic species. This approach represents a significant departure from traditional models in which the composition of seawater is parameterized in terms of only a few components or chlorophyll concentration alone. Because these simplified models are unable to predict the substantial variability in the optical properties observed in the ocean, advanced approaches such as the one described in this paper will be essential to furthering our understanding of ocean optics. Our approach allows us to investigate in detail how the various particulate components affect the bulk IOPs of seawater.

Our example simulations of the IOP model illustrate how the separation and understanding of the effects of various planktonic microorganisms and other particles present within a water body can be achieved. In the base simulation, which represents oligotrophic water with a chlorophyll concentration of 0.18 mg m^{-3}, the combined planktonic organisms are more important to light absorption than nonliving particles but their relative contribution to light scattering is significantly smaller. The picoplankton species are most important among planktonic components. Also, the plankton contribution to particulate backscattering is remarkably small, which is consistent with the conjecture derived in previous studies.[25,49] Note, however, that our estimates of the backscattering cross sections of microorganisms are subject to uncertainties associated with the use of Mie-scattering calculations for homogeneous spheres. Recent studies[50,51] suggest that phytoplankton can exhibit higher backscattering than estimated from Mie calculations. Further research is needed, especially direct measurements of backscattering on phytoplankton cultures.

Another result from the base simulation is that most scattering is due to minerals, which is especially well pronounced for backscattering. Significant scattering by minerals suspended in seawater was suggested earlier by Gordon.[52] Our results must be interpreted with caution because they depend strongly on the choice of the concentration of minerals used in the model simulation. We do not imply that mineral particles typically dominate scattering in the upper layers of the oligotrophic ocean. In fact, the optical effects of such particles have been generally considered to be negligible compared with organic particles in the open ocean. Our model simulations are, however, instructive because they indicate the potential role of minerals even if these particles are less abundant than organic particles. In this context note the large-scale aeolian transport of mineral dust to the world ocean. For example, mineral dust produced in the Saharan region has been shown to represent a considerable source of par-

ticles to the Atlantic and Mediterranean.[53,54] It is thus possible that minerals could be optically important not only in coastal waters but also occasionally in the open ocean, for example, during episodes of dust deposition. Clearly, the question of how the optical effects of mineral particles vary in the ocean needs further examination.

In the present example simulations cannot provide generalized conclusions about the roles played by various particles in ocean optics, but they show that this approach is a powerful research tool permitting the analysis of IOPs as the detailed composition of particulate assemblage is varied in a controlled manner as desired. In a series of bloom simulations we show that variations in the composition of planktonic community lead to significant variations in IOPs, although the chlorophyll concentration in the simulated water bodies remains unchanged. More extensive simulations of this kind promise better understanding of the optical effects of various particles and variability in bio-optical models that involve chlorophyll parameterizations. In addition, the combination of this approach with radiative-transfer modeling provides an ideal means of separating and understanding the effects of various components on light fields within and leaving water bodies.[20]

The improvements in our understanding of the optical variability in the ocean are currently hindered because routine measurements of the bulk optical properties of seawater offer little or nothing about the variable contributions associated with many individual components of seawater. Usually sufficient knowledge about the concentrations and optical properties of various types of particle present in any examined water body is not available. To take full advantage of the approach presented in this study, an increased effort to characterize the types and concentrations of particle suspended in seawater is needed. To succeed in this effort, coordinated research is required in which analyses of marine particles by advanced techniques (for example, flow cytometry and image-analyzed microscopy) are carried out in tandem with a comprehensive suite of optical measurements, both *in situ* and in the laboratory.

This research was supported by the Office of Naval Research Environmental Optics Program (D. Stramski) and the NASA Biogeochemistry Program (D. Stramski) in the United States, and the Centre National de la Recherche Scientifique (A. Bricaud and D. Stramski) and Université Pierre et Marie Curie (A. Morel) in France. We thank Y.-H. Ahn for his contributions to the study of the optical properties of phytoplankton, R. Iturriaga and D. Siegel for making data available from the microspectrophotometric analysis of detrital particles, and C. Mobley for helpful discussions of the study while it was in progress.

References

1. A. Morel and L. Prieur, "Analysis of variations in ocean color," Limnol. Oceanogr. **22,** 709–722 (1977).
2. R. C. Smith and K. S. Baker, "Optical classification of natural waters," Limnol. Oceanogr. **23,** 260–267 (1978).
3. H. R. Gordon and A. Morel, "Remote assessment of ocean color for interpretation of satellite visible imagery—a review," in *Lecture Notes on Coastal and Estuarine Studies*, R. T. Barber, C. N. K. Mooers, M. J. Bowman, and B. Zeitzschel, eds. (Springer-Verlag, New York, 1983).
4. A. Morel, "Optical modeling of the upper ocean in relation to its biogenous matter content (case I waters)," J. Geophys. Res. **93,** 10,749–10,768 (1988).
5. A. Bricaud, A. Morel, M. Babin, K. Allali, and H. Claustre, "Variations of light absorption by suspended particles with chlorophyll a concentrations in oceanic (Case 1) waters: analysis and implications for bio-optical models," J. Geophys. Res. **103,** 31,033–31,044 (1998).
6. H. Loisel and A. Morel, "Light scattering and chlorophyll concentration in case 1 waters: a reexamination," Limnol. Oceanogr. **43,** 847–858 (1998).
7. J. E. O'Reilly, S. Maritorena, B. G. Mitchell, D. A. Siegel, K. L. Carder, S. A. Garver, M. Kahru, and C. McClain, "Ocean color chlorophyll algorithms for SeaWiFS," J. Geophys. Res. **103,** 24,937–24,953 (1998).
8. N. G. Jerlov, *Marine Optics* (Elsevier, Amsterdam, 1975).
9. J. T. O. Kirk, *Light and Photosynthesis in Aquatic Ecosystems* (Cambridge University, Cambridge, England, 1994).
10. C. D. Mobley, *Light and Water. Radiative Transfer in Natural Waters* (Academic, San Diego, Calif., 1994).
11. R. P. Bukata, J. H. Jerome, K. Ya. Kondratyev, and D. V. Pozdnyakov, *Optical Properties and Remote Sensing of Inland and Coastal Waters* (CRC Press, Boca Raton, Fla., 1995).
12. A. Bricaud, A. Morel, and L. Prieur, "Absorption by dissolved organic matter of the sea (yellow substance) in the UV and visible domains," Limnol. Oceanogr. **26,** 43–53 (1981).
13. K. L. Carder, R. G. Stewart, G. R. Harvey, and P. B. Ortner, "Marine humic and fulvic acids: their effects on remote sensing of ocean chlorophyll," Limnol. Oceanogr. **34,** 68–81 (1989).
14. M. Kishino, M. Takahashi, N. Okami, and S. Ichimura, "Estimation of the spectral absorption coefficients of phytoplankton in the sea," Bull. Mar. Sci. **37,** 634–642 (1985).
15. C. S. Roesler, M. J. Perry, and K. L. Carder, "Modeling *in situ* phytoplankton absorption from total absorption spectra in productive inland waters," Limnol. Oceanogr. **34,** 1510–1523 (1989).
16. A. Bricaud and D. Stramski, "Spectral absorption coefficients of living phytoplankton and nonalgal biogenous matter: a comparison between the Peru upwelling area and Sargasso Sea," Limnol. Oceanogr. **35,** 562–582 (1990).
17. R. P. Bukata, J. H. Jerome, J. E. Bruton, S. C. Jain, and H. H. Zwick, "Optical water quality model of Lake Ontario 1. Determination of the optical cross sections of organic and inorganic particulates in Lake Ontario," Appl. Opt. **20,** 1696–1703 (1981).
18. R. P. Bukata, J. H. Jerome, K. Ya. Kondratyev, and D. V. Pozdnyakov, "Estimation of organic and inorganic matter in inland waters: optical cross sections of Lakes Ontario and Ladoga," J. Great Lakes Res. **17,** 461–469 (1991).
19. E. A. Gallie and P. A. Murtha, "Specific absorption and backscattering spectra for suspended minerals and chlorophyll *a* in Chilko Lake, British Columbia," Remote Sensing Environ. **39,** 103–118 (1992).
20. C. D. Mobley and D. Stramski, "Effects of microbial particles on oceanic optics: methodology for radiative transfer modeling and example simulations," Limnol. Oceanogr. **42,** 550–560 (1997).
21. R. M. Pope and E. S. Fry, "Absorption spectrum (380–700 nm) of pure water. II. Integrating cavity measurements," Appl. Opt. **36,** 8710–8723 (1997).
22. R. C. Smith and K. S. Baker, "Optical properties of the clearest natural waters (200–800 nm)," Appl. Opt. **20,** 177–184 (1981).
23. A. Bricaud, A.-L. Bedhomme, and A. Morel, "Optical properties

of diverse phytoplanktonic species: experimental results and theoretical interpretation," J. Plankton Res. **10,** 851–873 (1988).
24. D. Stramski and D. A. Kiefer, "Optical properties of marine bacteria," in *Ocean Optics X*, R. W. Spinrad, ed., Proc. SPIE **1302,** 250–268 (1990).
25. D. Stramski and D. A. Kiefer, "Light scattering by microorganisms in the open ocean," Prog. Oceanogr. **28,** 343–383 (1991).
26. Y.-H. Ahn, A. Bricaud, and A. Morel, "Light backscattering efficiency and related properties of some phytoplankters," Deep-Sea Res. **39,** 1835–1855 (1992).
27. A. Morel, Y.-H. Ahn, F. Partensky, D. Vaulot, and H. Claustre, "*Prochlorococcus* and *Synechococcus*: a comparative study of their optical properties in relation to their size and pigmentation," J. Mar. Res. **51,** 617–649 (1993).
28. D. Stramski and R. A. Reynolds, "Diel variations in the optical properties of a marine diatom," Limnol. Oceanogr. **38,** 1347–1364 (1993).
29. D. Stramski, G. Rosenberg, and L. Legendre, "Photosynthetic and optical properties of the marine chlorophyte *Dunaliella tertiolecta* grown under fluctuating light caused by surface wave focusing," Mar. Biol. **115,** 363–372 (1993).
30. D. Stramski, A. Shalapyonok, and R. A. Reynolds, "Optical characterization of the oceanic unicellular cyanobacterium *Synechococcus* grown under a day–night cycle in natural irradiance," J. Geophys. Res. **100,** 13,295–13,307 (1995).
31. C. F. Bohren and D. R. Huffman, *Absorption and Scattering of Light by Small Particles* (Wiley, New York, 1983).
32. A. Bricaud and A. Morel, "Light attenuation and scattering by phytoplanktonic cells: a theoretical modeling," Appl. Opt. **25,** 571–580 (1986).
33. D. Stramski and C. D. Mobley, "Effects of microbial particles on oceanic optics: a database of single-particle optical properties," Limnol. Oceanogr. **42,** 538–549 (1997).
34. E. J. Terrill, W. K. Melville, and D. Stramski, "Bubble entrainment by breaking waves and their effects on the inherent optical properties of the upper ocean," at Ocean Optics XIV Conference, Kailua-Kona, Haw, 10–13 November 1998, Ocean Optics XIV CD ROM (Office of Naval Research, Washington, D.C., 1998).
35. R. Iturriaga and D. A. Siegel, "Microspectrophotometric characterization of phytoplankton and detrital absorption properties in the Sargasso Sea," Limnol. Oceanogr. **34,** 1706–1726 (1989).
36. W. G. Egan and T. W. Hilgeman, *Optical Properties of Inhomogeneous Materials. Applications to Geology, Astronomy, Chemistry, and Engineering* (Academic, New York, 1979).
37. I. N. Sokolik and O. B. Toon, "Incorporation of mineralogical composition into models of the radiative properties of mineral aerosol from UV to IR wavelengths," J. Geophys. Res. **104,** 9423–9444 (1999).
38. K. L. Carder, P. R. Betzer, and D. W. Eggimann, "Physical, chemical, and optical measures of suspended-particle concentrations: their intercomparison and application to the West African Shelf," in *Suspended Solids in Water*, R. J. Gibbs, ed. (Plenum, New York, 1974), pp. 173–193.
39. P. F. Kerr, *Optical Mineralogy* (McGraw-Hill, New York, 1977).
40. M. Jonasz and G. Fournier, "Approximation of the size distribution of marine particles by a sum of lognormal functions," Limnol. Oceanogr. **41,** 744–754 (1996).
41. S. Vagle and D. M. Farmer, "The measurement of bubble-size distributions by acoustical backscatter," J. Atmos. Ocean. Technol. **9,** 630–644 (1992).
42. L. M. Proctor and J. A. Fuhrman, "Viral mortality of marine bacteria and cyanobacteria," Nature (London) **342,** 60–62 (1990).
43. R. Maranger and D. F. Bird, "Viral abundance in aquatic systems: a comparison between marine and fresh waters," Mar. Ecol. Prog. Ser. **121,** 217–226 (1995).
44. M. Takahashi and P. K. Bienfang, "Size structure of phytoplankton biomass and photosynthesis in subtropical Hawaiian waters," Mar. Biol. **76,** 203–211 (1983).
45. P. G. Davis, D. A. Caron, P. W. Johnson, and J. M. Sieburth, "Phototrophic and apochlorotic components of picoplankton and nanoplankton in the North Atlantic: geographic, vertical, seasonal, and diel distributions," Mar. Ecol. Prog. Ser. **21,** 15–26 (1985).
46. B. C. Cho and F. Azam, "Biogeochemical significance of bacterial biomass in the ocean's euphotic zone," Mar. Ecol. Prog. Ser. **63,** 253–259 (1990).
47. W. K. W. Li, P. M. Dickie, B. D. Irwin, and A. M. Wood, "Biomass of bacteria, cyanobacteria, prochlorophytes, and photosynthetic eukaryotes in the Sargasso Sea," Deep-Sea Res. **39,** 501–519 (1992).
48. W. K. W. Li, "Composition of ultraphytoplankton in the central North Atlantic," Mar. Ecol. Prog. Ser. **122,** 1–8 (1995).
49. A. Morel and Y.-H. Ahn, "Optics of heterotrophic nanoflagellates and ciliates. A tentative assessment of their scattering role in oceanic waters compared to those of bacterial and algal cells," J. Mar. Res. **49,** 177–202 (1991).
50. J. Piskozub and D. Stramski, "The use of scattering error in absorption measurement for estimating the scattering phase function of marine phytoplankton," Program and Abstracts, Ocean Optics XV Conference, Musée Océanographique, Monaco (2000), p. 90.
51. R. D. Vaillancourt, C. Brown, and R. R. L. Guillard, "A taxonomic survey of the optical properties of marine phytoplankton with special emphasis on the backscattering coefficient," Earth Observing Syst. Trans. Am. Geophys. Union **80**(**49**), 119–120 (2000).
52. H. R. Gordon, "Mie theory of light scattering by ocean particulates," in *Suspended Solids in Water*, R. J. Gibbs, ed. (Plenum, New York, 1974), pp. 73–86.
53. K. L. Carder, R. G. Steward, P. R. Betzer, and J. M. Prospero, "Dynamics and composition of particles from aeolian input event to the Sargasso Sea," J. Geophys. Res. **91,** 1055–1066 (1986).
54. M. D. Loÿe-Pilot, J. M. Martin, and J. Morelli, "Influence of Saharan dust on the rain acidity and atmospheric input to the Mediterranean," Nature (London) **321,** 427–428 (1986).